STRUCTURAL AND TRANSCRIPTIONAL FEATURES OF THE MOUSE SPERMATID GENOME

A. L. KIERSZENBAUM and LAURA L. TRES

From the Department of Anatomy and Laboratories for Reproductive Biology, University of North Carolina, Chapel Hill, North Carolina 27514

ABSTRACT

A whole-mount electron microscope technique has allowed direct visualization of the transcription process in mouse spermatids. These observations have been supported by light and electron microscope autoradiographic techniques that employ [^{3}H]uridine and [^{3}H]arginine in attempts to clarify mechanisms of RNA synthesis and their relationship to nuclear histone changes throughout spermiogenesis. Early spermatid genomes are dispersed almost completely, whereas in later spermiogenic steps the posterior or flagellar nuclear region is readily dispersed and the anterior or subacrosomal nuclear region remains compact. Display of genome segments permits identification of regions where transcription complexes, presumably heterogeneous nuclear RNA species, are seen related to chromatin. These complexes appear as ribonucleoprotein chains, some of them of considerable length, decreasing progressively in number in late spermiogenic steps. This decrease coincides with diminishing rates of [^{3}H]uridine incorporation. Two distinct patterns of chromatin have been identified: a *beaded chromatin type* associated with transcription complexes encountered in early spermatids; and a *smooth chromatin type* not involved in transcriptive activity observed in advanced spermiogenic genomes. Protein particles staining densely with phosphotungstic acid become apparent in nuclei of spermatids after [^{3}H]arginine incorporation becomes significant. There is no structural or autoradiographic evidence for the presence of nucleoli during spermiogenesis. From these data and from previous experimental findings, we conclude that: (*a*) spermatogonia, spermatocytes and Sertoli cells are transcriptionally expressed into heterogeneous nuclear RNA and preribosomal RNA species whereas transcription in spermatids is predominantly heterogeneous nuclear RNA; and (*b*) the modification of the chromatin patterns in late spermiogenic steps indicates a stabilized genome that restricts transcriptive functions.

Spermatogenesis in mammals is a highly synchronous process characterized, among other events, by regular temporal variations in the amount of transcription at various loci of the constituent genomes. Several aspects of RNA synthesis in meiotic prophase stages in the mouse have been described recently (15). In that study we reported evidence for two major classes of RNA associated with autosomes in synapsis: a preribosomal RNA (prRNA) located at the terminal or basal knob region of some autosomes, and a heterogeneous nuclear RNA (hnRNA) distributed along the

margins of bivalents. Furthermore, precise localization of rapidly labeled RNA was obtained by displaying the total set of bivalents (autosomes and sex chromosomes) of mouse pachytene spermatocytes by use of whole-mount electron microscope procedures combined with autoradiography (16). Moreover, we demonstrated a lampbrush organization of bivalent autosomes as well as the presence of nascent ribonucleoprotein (RNP) chains, probably representing hnRNA molecules attached at intervals to chromatin loops.

These findings have stimulated our interest in exploring the capabilities of the spermatid haploid genome for transcribing RNA until it is released at spermiation from its Sertoli cell association. Much has been learned of the morphogenesis of the acrosome, of nuclear shaping, and of sperm tail elements in several species from electron microscope study of sections (9, 31). Despite many efforts to determine structural changes and functional events which occur during nuclear condensation, our understanding of the spermatid nuclear structure is still incomplete. Data on RNA synthesis in the mouse testis obtained from light microscope autoradiographic localization of [^{3}H]uridine incorporation (26) and from an assay system for localization of endogeneous RNA polymerase activity (27) indicate that postmeiotic transcription occurs in early steps of spermiogenesis but not in later steps, when it is no longer possible to detect the presence or synthesis of RNA.

As mammalian spermatids differentiate to become spermatozoa, the DNA-associated "somatic" histone is apparently replaced by a more basic arginine-rich protein (2, 25). In the mouse this replacement coincides with a high [^{3}H]arginine labeling rate, detectable in advanced spermatids and even in the head of mature sperm (25). In this respect, Lam and Bruce (19) have reported extraction of a protein which is highly basic and arginine- and lysine-rich, but free of cysteine (mouse "protamine") from physically separated cells of the mouse testis. The amino acid composition of this protein differs from that of fish (8) and spermatozoa proteins (6, 22) from other mammalian species.

In this paper we report studies of the nuclear organization of mouse spermatids with special reference to changes in the structure and arrangement of genome segments, some of them related to transcription. This study has been facilitated by a procedure for visualization in the electron microscope of transcription developed by Miller and Bakken (24) and adapted for the testis by Kierszenbaum and Tres (16). The method readily dispersed the chromatin of spermatid nuclei. We also report labeling experiments with [^{3}H]uridine combined with electron microscope autoradiography. These indicate rapidly labeled (hnRNA) transcriptive species predominant in early spermatids. In addition, we show the localization of [^{3}H]arginine as displayed by light microscope autoradiography at different spermiogenic steps.

MATERIALS AND METHODS

Adult male Swiss mice (45–60 days old) were anesthetized with ether before injection of [5,6-^{3}H]uridine (sp act 42.4 Ci/mmol) and L-[3-^{3}H]-*N*-arginine (sp act 27.3 Ci/mmol, both from New England Nuclear, Boston, Mass.) to label RNA and proteins, respectively. The labeled precursors were injected directly into both testes under the albuginea at a dose of 10 μCi for [^{3}H]uridine and 15 μCi for [^{3}H]arginine per testis in a vol of 0.05 ml of sterile water. Testes were removed under anesthesia at the following [^{3}H]uridine postinjection intervals: 5, 15, 30, and 60 min; 3 and 24 h; 7, 8, 10, and 12 days; and after a single [^{3}H]arginine injection interval of 60 min. The reasons for selecting an intratesticular route for isotope injection are discussed elsewhere (15).

Electron Microscope Visualization of Transcription in the Testis

We used the method described by Miller and Bakken (24) for the visualization of transcription in mammalian cells after adapting it for the mouse testis. Testes were removed under anesthesia and placed on a watch glass kept on crushed ice. The tunica albuginea was removed. The seminiferous tubules were resuspended either in cold isotonic saline or in distilled water and the cells were dissociated from the seminiferous tubules by repeated aspirations and ejections with a syringe. The suspension was transferred to centrifuge tubes (15 ml) precooled in ice and was centrifuged at 800 *g* for 3 min. The supernate was discarded and the pellet resuspended in fresh isotonic saline or in distilled water with a Pasteur pipet. A drop of the cell suspension was allowed to disperse for 3–5 min in a cold 0.3% solution of the detergent Joy (Proctor & Gamble, Cincinnati, Ohio). The dispersed nuclear material was centrifuged (2,350 *g*, 5 min) through a neutral solution of 0.1 M sucrose with 10% Formalin onto hydrophilic carbon-coated electron microscope grids (300 mesh). Formvar-carbon-coated grids (150 mesh) were also used, with good results. The grids were rinsed in 0.4% Kodak Photo-flo (Eastman Kodak Co., Rochester, N. Y.) and air dried. Preparations were stained with 1% phosphotungstic acid in 95% ethanol at pH 2.5, rinsed in 95% ethanol, and air dried. Some grids were stained with 1% uranyl acetate in 95% ethanol and then with phosphotungstic acid as described above.

Autoradiographic Techniques for Light Microscopy

Sections 0.5 μm thick of tissue embedded in Maraglas (Polysciences, Inc., Rydal, Pa.) were deposited on glass slides and dipped in undiluted Kodak NTB3 emulsion. After exposure for 25–30 days at 4°C, the preparations were developed in Kodak D-19 for 30 s and fixed in Kodak Rapid Fixer for 2 min. Sections were stained through the emulsion with 1% toluidine blue in 1% sodium borate for 3 min at 40°C.

Autoradiographic Techniques for Electron Microscopy

Thin sections of seminiferous tubules fixed in glutaraldehyde-osmium tetroxide were transferred to parlodion-coated half glass slides split lengthwise. Before being coated with emulsion, the sections were stained with uranyl acetate and lead citrate. A thin carbon layer was vacuum evaporated over the stained sections, and the slides were dipped in a diluted Ilford L4 emulsion (Ilford, Ltd., Ilford, Essex, England). After exposure for 25 days–5 mo, the preparations were developed with the gold latensification-Elon ascorbic acid procedure (33). Fixation was carried out with Kodak Rapid Fixer for 1 min. After a rinsing in distilled water, the specimens were stripped off onto a water surface and copper electron microscope grids were placed over the sections and picked up with a Parafilm strip (American Can Co., Neenah, Wis.).

For whole-mount nuclei, a drop of a suspension of mouse testicular cells labeled with [^{3}H]uridine was spread on a surface of 0.9% aqueous NaCl, picked up on electron microscope grids supporting a Formvar-carbon film, and stained in uranyl acetate. A monolayer of Ilford L4 emulsion was applied to the grids by a wire loop. After an exposure time of 30–60 days, specimens were developed with the gold latensification Elon-ascorbic acid procedure for filamentous grains (34), fixed with Kodak Fixer, rinsed in distilled water, and air dried.

Specimens were examined in a JEM 100B electron microscope with a "cool beam" gun system operated at 60, 80, or 100 kV with an objective aperture of 50 μm diameter. Measurements were made from enlarged photographs at convenient sizes, using for calibration an electron micrograph of copper phthalocyanine crystal lattice with spacings of 1.26 nm.

RESULTS

Structure of the Spermatid Genome

For correlating structural transitions during spermatid development we found it convenient to identify 16 successive spermiogenic steps in the mouse testis, which can in turn be divided into three main groups: the *early spermatid* (corresponding approximately to steps 1–8); the *elongating spermatid* (approximately steps 9–12); and the *late spermatid* (steps 13–16) (see Fig. 13). This classification is based on changes in nuclear shape and condensation as described by Oakberg (29) and Monesi (25).

Identification of early spermatids in whole-mount electron microscope preparations is facilitated by the preservation of the acrosome, which remains firmly attached to the dispersed nucleus. Late spermatids are recognized by their characteristic nuclear shape.

It is well known that late spermatid nuclei are usually devoid of resolvable fine structure when observed in thin sections with the electron microscope. When these nuclei are prepared for whole-mount electron microscopy after a brief detergent treatment for 3–5 min at 4°C, a decondensation of the nucleus is achieved to a degree permitting some structural information to be obtained. This treatment detaches most flagella from spermatid heads.

Late spermatid nuclei are only partly dispersed by this procedure. The posterior portion of the nucleus near the flagellar attachment is adequately dispersed, whereas the anterior subacrosomal nuclear region remains fully condensed (Fig. 1). These results agree with similar findings on the nuclear decondensation induced by sodium dodecyl sulfate and dithiothreitol in different mammalian spermatozoa isolated from the epididymis (5).

The subacrosomal nuclear region contains many coarse aggregates of dense particles which bind phosphotungstic acid (PTA) at pH 2.5 (Fig. 1). Clustered particles of comparable size and shape but of less electron density lie within the dispersed posterior flagellar nuclear region (Fig. 2). We interpret the nature of the dense particulate material in the light of Silverman and Glick's (35) observations that PTA binds to proteins in acid solution to form dense complexes. In the spermatid head we are tempted to speculate that the binding of PTA to the particles may indicate arginine-rich proteins forming during elongation of spermatids in later spermiogenic steps. This process coincides with a progressive nuclear condensation and increased [^{3}H]arginine uptake. In support of this interpretation, our light microscope autoradiograms of seminiferous tubules show a predominant nuclear labeling of late spermatids fixed 60 min after [^{3}H]arginine administration, whereas in the same preparations, early and elongating spermatids are only lightly labeled (Figs.

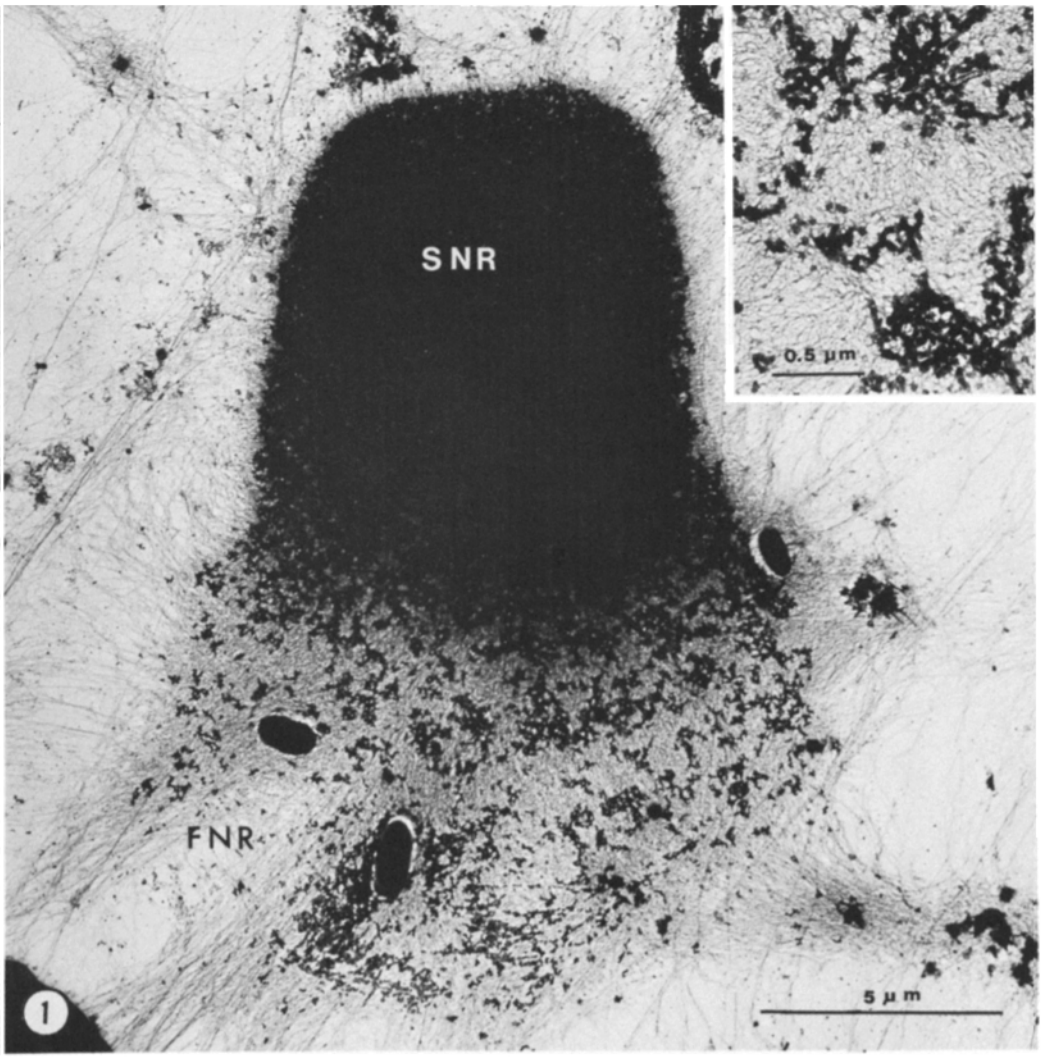

FIGURE 1 Electron micrograph of a dispersed nucleus of a late spermatid of mouse testis. The anterior or subacrosomal nuclear region (*SNR*) remains compact, contrasting with a well-dispersed posterior or flagellar nuclear region (*FNR*). Chromatin fibers spread out from the disrupted nucleus. × 6,750. *Inset*, Detail of a nuclear region with dense particles interspersed among chromatin fibers. × 25,600. This spermatid head was lysed and dispersed by detergent solution at about 4° C for 3 min (pH 8.2), centrifuged onto a carbon-coated electron microscope grid, and positively stained for 1 min in 1% alcoholic phosphotungstic acid (see Materials and Methods for details).

10, 11). It should be noted, however, that pachytene spermatocytes (Fig. 11) are also heavily labeled with [^{3}H]arginine long before protamines are synthesized. Biochemical observations indicating a high content of arginine-rich proteins at these spermiogenic steps (17, 19, 22) provide support for the assumption that the dense particulate material which binds PTA may correspond to arginine-rich proteins. However, the ultimate test for the exact nature of these particles must be derived from additional electron microscope autoradiograms and enzymatic studies.

Electron micrographs of dispersed mouse spermatid genomes display two different structural types of chromatin: a type formed by bundles of smooth chromatin fibers interconnected by bridging chromatin fibers, and another chromatin type showing a beaded appearance produced by sphe-

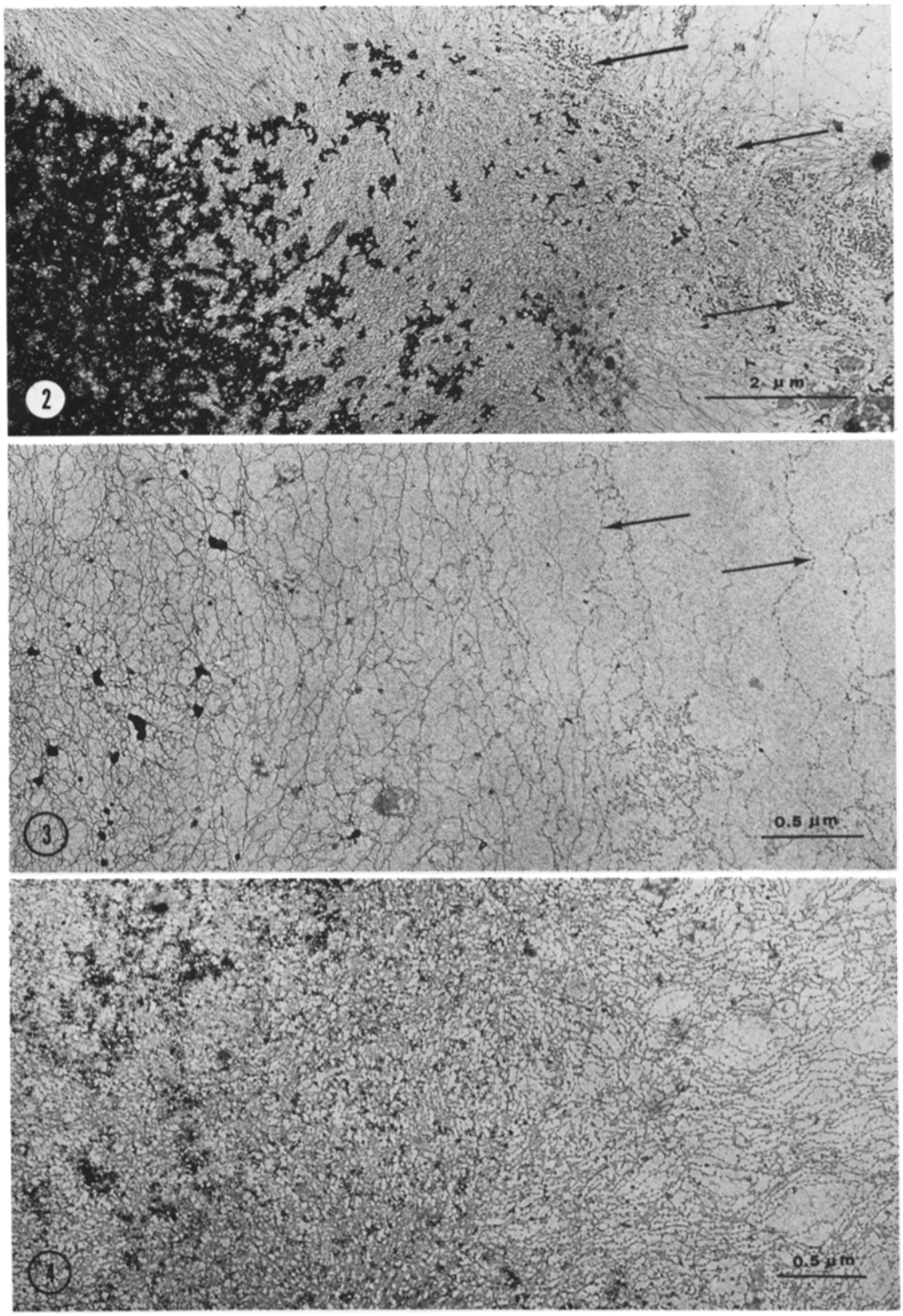

FIGURE 2 Late spermatid mouse genome at flagellar nuclear region, showing a gradient of dense structures. Arrows indicate clustered small particles. × 12,000.

FIGURE 3 Late spermatid mouse genome at flagellar nuclear region. Smooth chromatin fibers in a network display are related to dense particles. Beaded chromatin fibers are identified in this nuclear region. × 33,300.

FIGURE 4 Elongating spermatid of a mouse. Chromatin fibers are predominantly of the beaded type. Dense particles are smaller than in Figs. 2 and 3. × 28,000.

roidal molecular particles, 6–9 nm in diameter, connected by thin strands 1.5–2 nm wide, aligned along the chromatin fiber (Fig. 7 *a*) forming a "flexible jointed chain" (18). The first or smooth type of chromatin is predominant in late spermatid genomes (Figs. 1–3 and 7), whereas the beaded type is characteristic of earlier spermiogenic steps (Fig. 4). A detailed display of both types of chromatin is depicted in Fig. 7.

Transcriptive Activity of the Spermatid Genome

During spermiogenesis in the mouse and in other mammals, RNA synthesis ceases before the time of nuclear condensation (26, 36). We have recently reported (15) that early spermatids show nuclear incorporation of tritiated RNA precursor 15 min after injection of [^{3}H]uridine. Fig. 13 indicates nuclear silver grain values at various steps of spermiogenesis obtained from electron microscope autoradiograms of mouse testicular material with a [^{3}H]uridine pulse of 3 h. An autoradiogram of a very early spermatid (presumably step 1 or 2) shows scattered silver grains in the nucleoplasm after a [^{3}H]uridine labeling of 3 h (Fig. 9). A large condensed centrally located chromatin structure displays silver grains at its margins. Other dense round-shaped elements are devoid of labeling. An elongating spermatid nucleus (approximately step 8 or 9) shows similar labeling features except that it lacks intranuclear dense masses (Fig. 8). After 8 days of labeling, no silver grains have been detected in the mature spermatid head. In a whole-mount autoradiographic preparation of spread early spermatid labeled with [^{3}H]uridine, silver grains are related mainly to dispersed chromatin fibers (Fig. 12).

We have previously described features of nascent RNP chains attached to chromatin loops of lampbrush autosomal bivalents in pachytene spermatocytes and have related them to template products being transcribed into hnRNA (16). In Fig. 6, active chromatin segments of the beaded type of chromatin belonging to an early spermatid genome are seen next to tangled RNP chains of

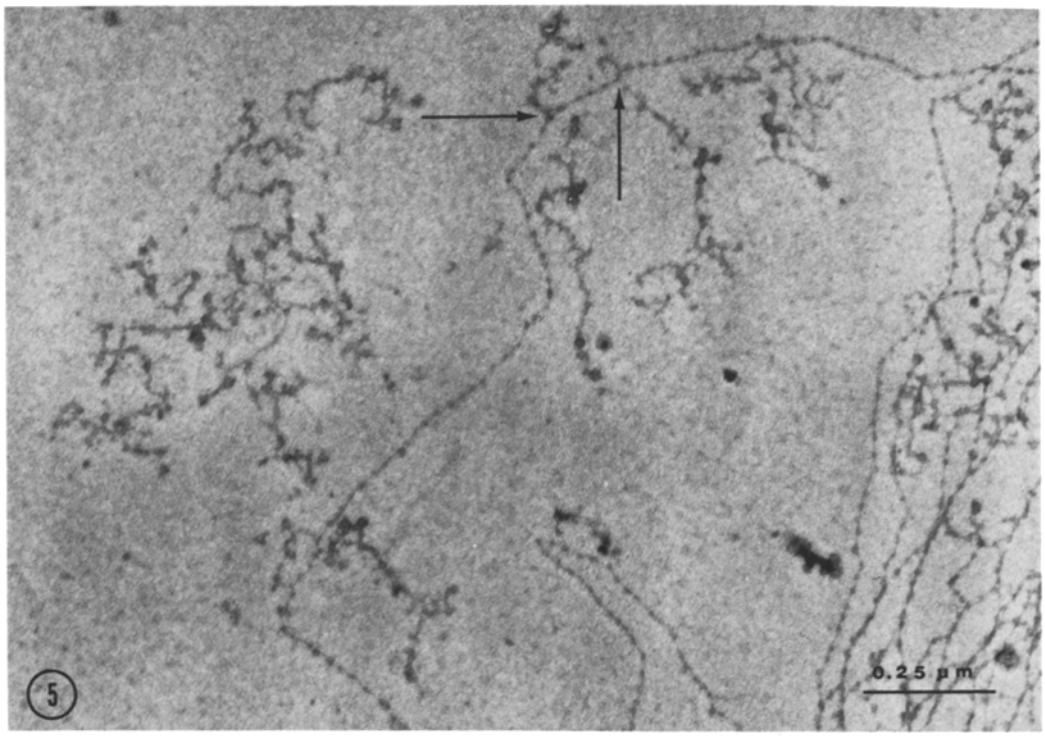

FIGURE 5 Electron micrograph of an active chromatin loop of a pachytene spermatocyte autosomal bivalent. RNP fibrils of different length are both free in the nucleoplasm and attached (arrows) to the chromatin fiber. × 73,500.

considerable length. Two features noted in early spermatid genomes deserve comment. Nascent RNP fibrils in early spermatids are quite far apart along genome segments, suggesting that transcriptive initiation sites are widely spaced. In addition, such large transcriptional complexes, as seen in Fig. 6, suggest a high molecular weight for the nascent RNA. For comparison, Fig. 5 illustrates transcription in a loop of an autosomal bivalent (mouse pachytene spermatocyte). The origins of nascent RNP fibers are closer than in spermatids, indicating more frequent initiation points of RNA synthesis either at a given locus or at more closely spaced loci in spermatocytes. The short length (about 1.35 μm) of the chromosomal segment between the very long RNP fibers in Fig. 5 would suggest that they are transcripts of the same DNA sequence. Structural details of these RNP complexes differ slightly from those described by us using a liquid-air interface spreading method (16), perhaps due to adverse effects of detergent on RNP.

DISCUSSION

The fine structural organization of the mouse spermatid genome has been studied throughout spermiogenesis and correlated with light and electron microscope autoradiography of [^{3}H]uridine and [^{3}H]arginine that serve as precursors for RNA and arginine-rich sperm histone and other proteins containing arginine.

Correlations between structure and labeling experiments indicate that transcription occurs in immature spermatid nuclei and decreases as the genome condenses to a significant degree. This decrease in transcription in late spermatid coincides with changes in the structure of chromatin fibers, the accumulation of coarse protein aggregates, and increasing rates of [^{3}H]arginine incorporation. Several observations suggest that RNA transcribed at initial spermiogenic steps is mainly of the hnRNA type that is newly synthesized on the haploid genome. Among these is the diffuse nucleoplasmic [^{3}H]uridine labeling in early spermatids detected by electron microscope autoradiographic procedures in thin sections and in whole-mount spread preparations, together with the widely spaced RNP chains associated with chromatin segments. Autoradiographic observations do not support a nucleolar organization in mouse spermiogenesis. Since nucleoli are important sources of prRNA in eukaryotes, it is possible to assume that spermatid genomes are mainly involved in the transcription of high molecular weight RNA (hnRNA).

It is now possible to integrate our autoradiographic findings on RNA synthesis in mouse seminiferous epithelium by concluding that Sertoli cells (14, 15), spermatocytes (15, 16), and spermatogonia (Tres and Kierszenbaum, unpublished observations) transcribe both hnRNA and prRNA, whereas early spermatid nuclei contain predominantly hnRNA species. The finding of a nucleolar RNA synthesis in spermatocytes disagrees with a recent hypothesis proposing a ribosomal RNA transfer from spermatogonia to spermatocytes mediated by Sertoli cells (10).

Electron microscope studies of whole-mount late spermatids (amphibian) and spermatozoan (fish and mammals) heads dried with the Anderson critical point method (20, 21, 38) have indicated that nuclei contain fibrillar chromatin and that condensed spermatozoa nuclei arise from aggregations of chromatin fibers. Moreover, coarse granules with large diameters have been described in thin sections during cat spermiogenesis (4). It is apparent from our observations on late spermatids that electron-dense nuclear particles are closely related to chromatin. Although, as previously noted, the chemical nature of these particles remains to be elucidated, we assume that they are rich in basic proteins. In this respect, Lam and Bruce (19) have reported a mouse "protamine" in mouse spermatids. A similar spermatid-specific basic protein has been reported in the rat testis by Kistler et al. (17). Marushige and Marushige (23) reported a sperm histone in the condensed chromatin fraction of rat testes. This condensed chromatin fraction which probably contains elongating and late spermatids differs from another soluble chromatin fraction corresponding to early spermatids which are devoid of sperm histone (23).

We have studied the structure of dispersed genome segments throughout spermiogenesis in an effort to visualize directly the transcription process already recognized from [^{3}H]uridine labeling patterns of sectioned early spermatids. The essential facts are related to variations in chromatin structure displayed by the procedure of Miller and Bakken (24) for visualization of genetic activity. Two distinctive structural types of chromatin fibers have been recognized: a beaded chromatin type observed in early spermiogenic steps and related to nascent RNP; and a smooth chromatin

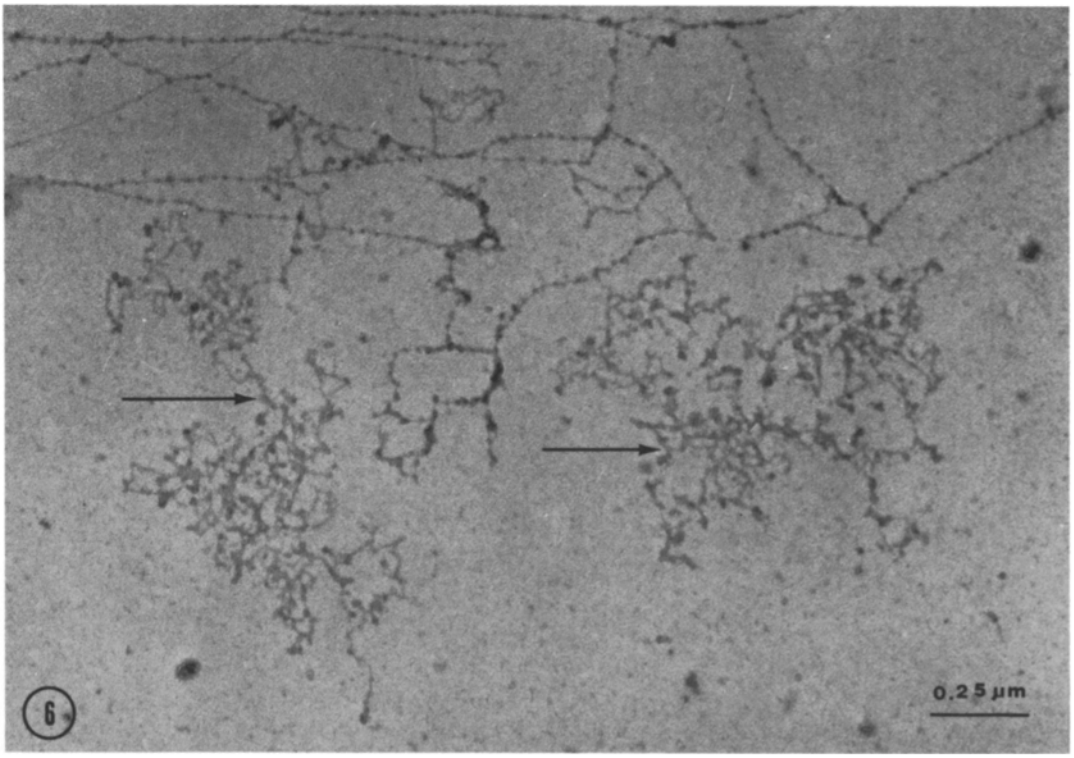

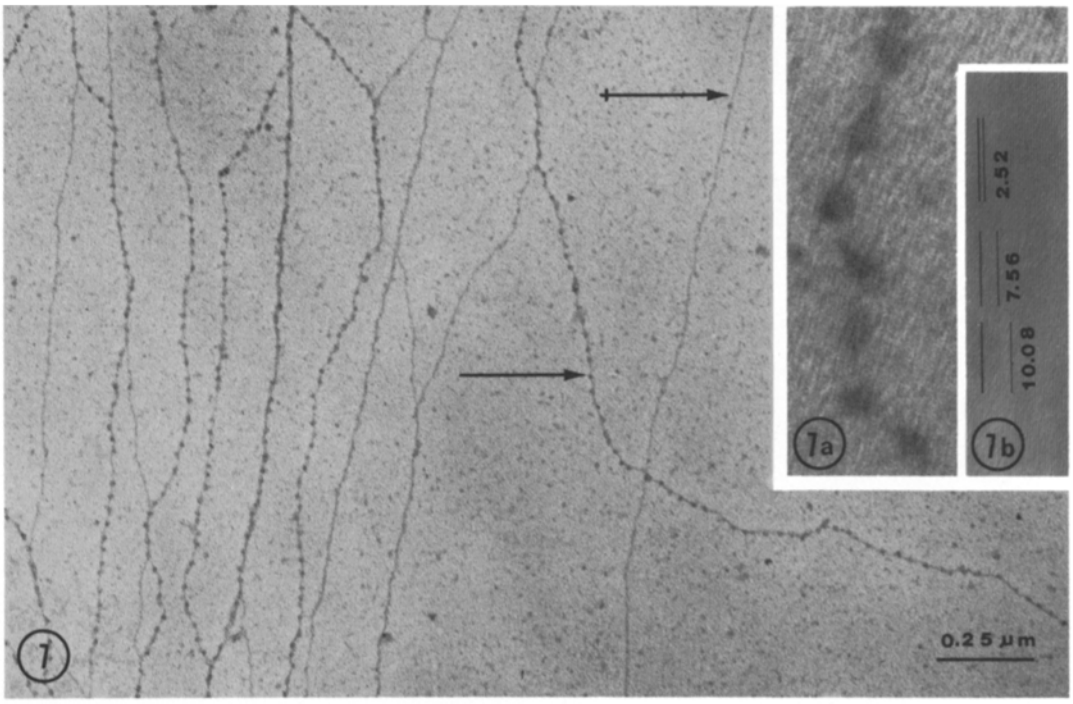

FIGURE 6 Electron micrograph of active genome segments of an early spermatid displaying RNP complexes of considerable length presumably representing hnRNA molecules (arrows). × 57,800.

FIGURE 7 Electron micrograph of beaded (arrow) and smooth (crossed arrow) chromatin fibers in a mouse spermatid. The different association of chromatin fibers creates "Y"-shaped branchings. × 57,800. Fig. 7 *a*. Beaded type of chromatin. × 400,000. Fig. 7 *b*. Copper phthalocyanine crystal lattice. × 400,000. Spacings in nanometers are indicated for estimation of chromatin particle size. Diameters of these particles and the length of connecting thin filaments are probably influenced by stretching during the preparative procedure (see reference 30 for an analysis of measurement values).

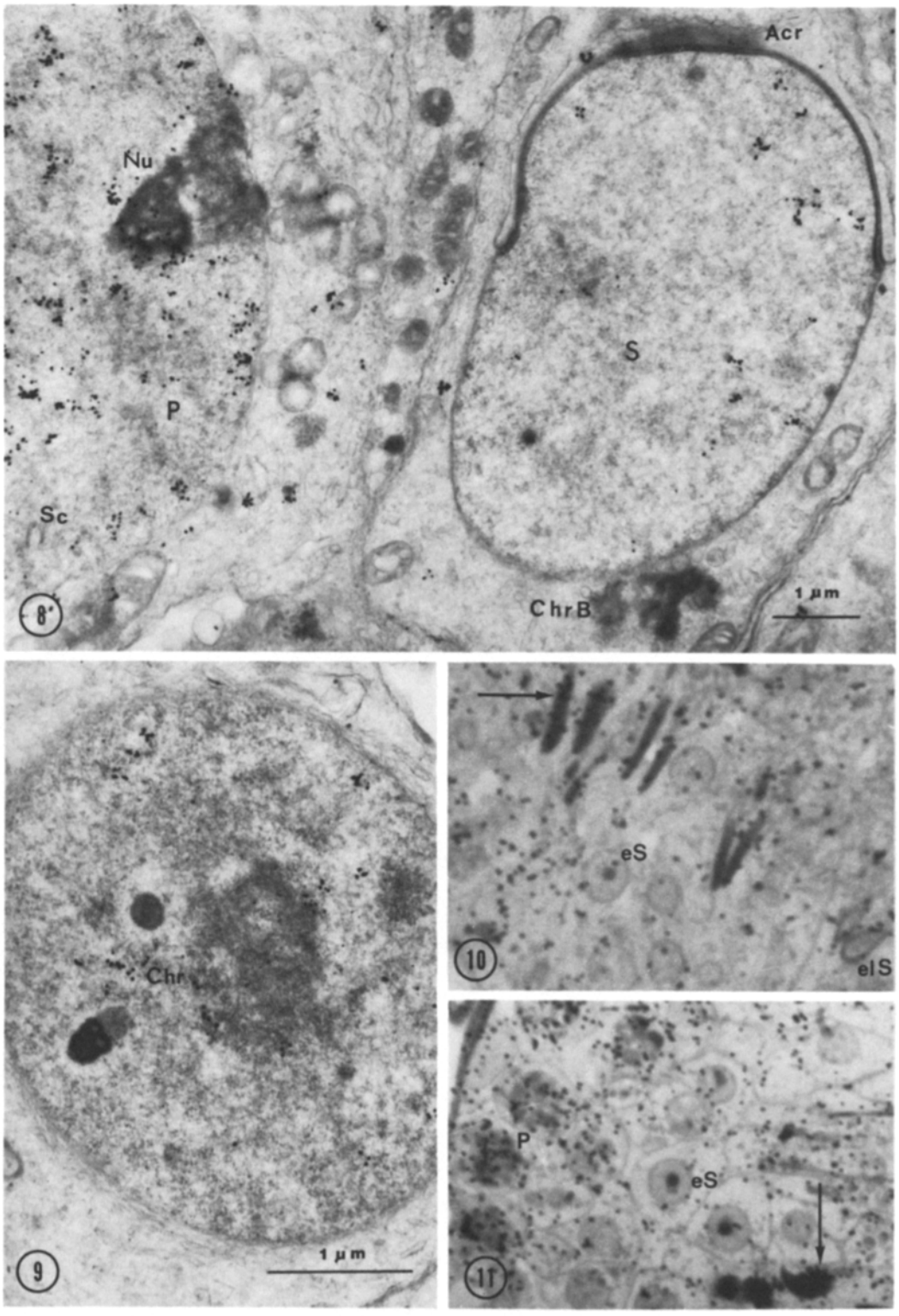
Acr
Nu
S
P
Sc
ChrB
1 µm
8'
9
Chr
1 µm
10
eS
elS
11
P
eS

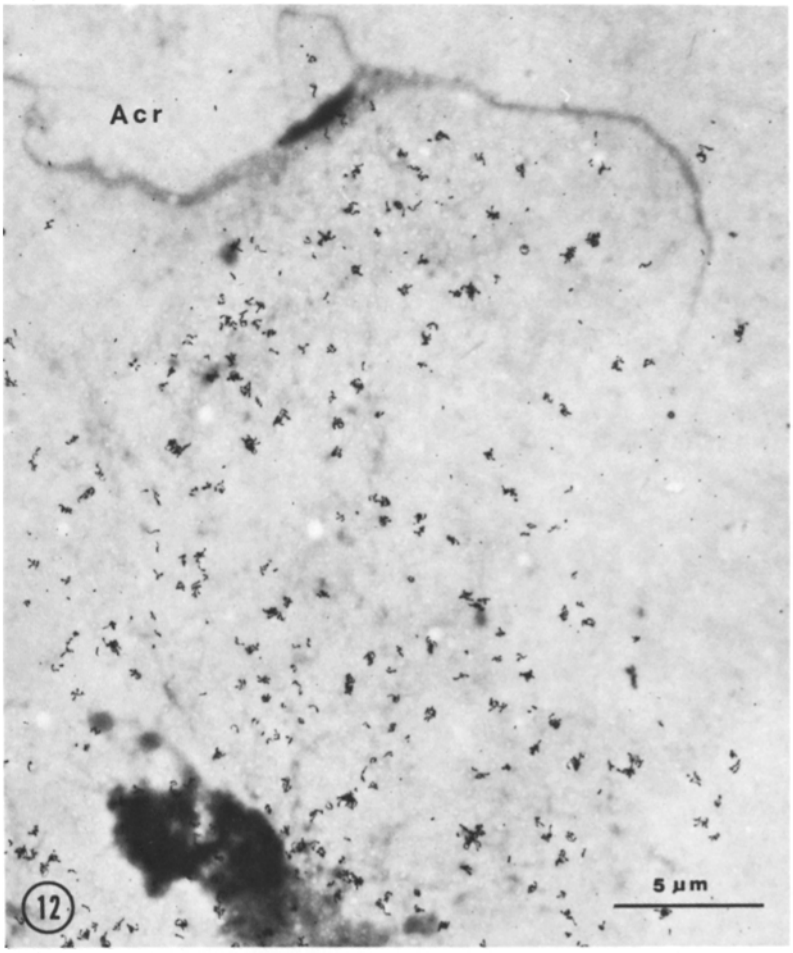

FIGURE 12 Electron microscope autoradiogram of a whole-mount spread of early spermatid. Labeling: [^{3}H]uridine, 3 h. Exposure time: 45 days. Developing procedure: gold latensification-Elon ascorbic acid procedure for filamentous silver grains. Although our whole-mount preparations yield insufficient resolution for a precise characterization of chromatin fibers, it is possible to assume that the even silver grain density is related to dispersed genome segments. *Acr*, acrosome. × 3,900.

FIGURE 8 Electron microscope autoradiogram of mouse seminiferous epithelium. Labeling: [^{3}H]uridine, 3 h. Exposure time: 60 days. Developing procedure: gold latensification-Elon ascorbic acid method. Sparse nucleoplasmic silver grains in an elongating spermatid (*S*) contrast with abundant nucleoplasmic grains in a pachytene spermatocyte (*P*). *Acr*, acrosome; *ChrB*, unlabeled chromatoid body; *Nu*, nucleolus; *Sc*, synaptonemal complex. × 13,600.

FIGURE 9 Electron microscope autoradiogram of an early spermatid (presumably step 1 or 2). Labeling, exposure time, and developing procedure as in Fig. 8. A large chromatin-condensed structure (*Chr*) displays marginal silver grains. The other dense structures remain unlabeled. Some silver grains are seen in the nucleoplasm. × 22,800.

FIGURE 10 Light microscope autoradiogram of mouse seminiferous tubule. Labeling: [^{3}H]arginine, 60 min. Exposure time: 14 days. Developing procedure: developer Kodak D-19. Late spermatid nuclei are well labeled (arrow). Early (*eS*) and elongating (*elS*) spermatids display some silver grains. × 5,400.

FIGURE 11 Same as Fig. 10. Pachytene spermatocyte (*P*) labeling with [^{3}H]arginine contrasts with almost unlabeled early spermatids (*eS*). Late spermatids are labeled (arrow). × 4,600.

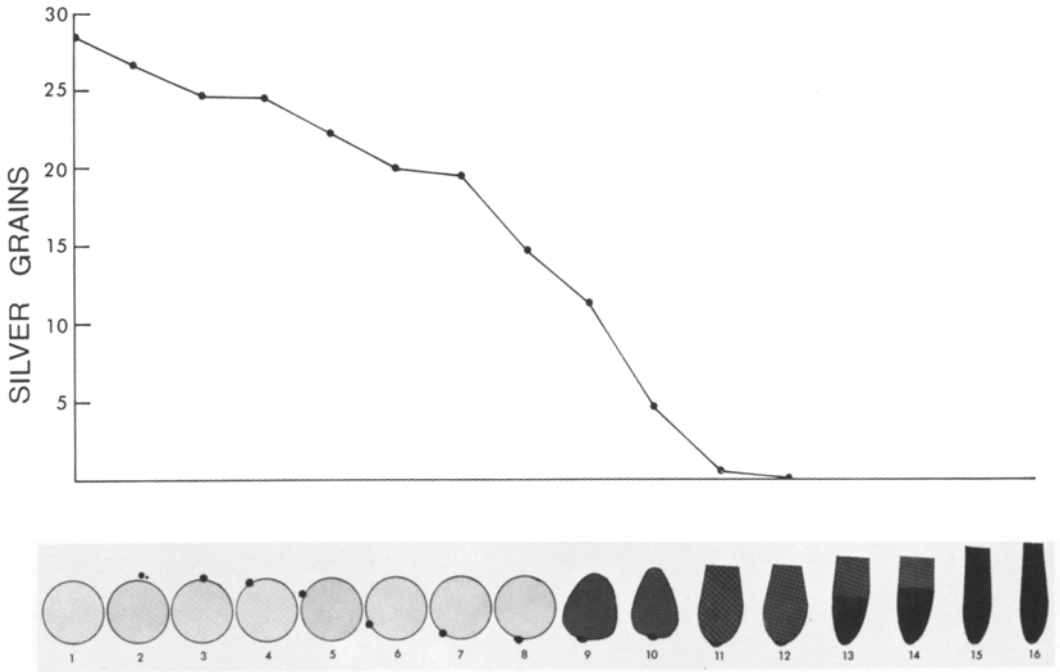

FIGURE 13 Diagram illustrating the nuclear incorporation of [^{3}H]uridine throughout different spermiogenic steps in the mouse after a pulse labeling of 3 h. Data were obtained by scoring 50 cells per spermiogenic step in light microscope autoradiograms. Each point in the graph expresses mean values. Ordinate indicates the number of silver grains per nucleus; abscissa represents changes in shape and condensation of nuclei throughout 16 spermiogenic steps. Numbers indicate those steps.

type, widespread in later spermiogenic steps in which transcription is declining or absent. This smooth chromatin type tends to associate with adjacent smooth threads of the same type and, less frequently, with the beaded fiber. This particular finding presumably accounts for the variable diameters of chromatin fibers and branching points observed by Lung (21) in human spermatozoa.

Electron microscope features of eukaryotic chromatin consisting of repeating units in a linear array have been presented recently (30). Kornberg (18), and Olins and Olins (30) have proposed models in which chromatin subunits are composed of histone molecules complexed with a double-stranded DNA. The subunit chromatin model has been supported by nuclease digestion experiments indicating that 85% of chromatin can be cleaved to integral subunit multiples (28).

The above-indicated relationship of the beaded chromatin type with an active template function agrees with similar features depicted by Miller and Bakken (24) and Hamkalo and Miller (12) in electron micrographs of transcription in several eukaryotic genomes. In fact, this subunit chromatin type is not seen in *Escherichia coli* (prokaryote) active genome regions (i.e., Fig. 6 *a*, *b* in reference 12) where more than 90% of the protein corresponds to RNA polymerase (37) and histone is not present.

We assume that both the smooth chromatin pattern and its associative behavior in advanced spermiogenesis are related to a gradual increase in stability of the deoxyribonucleo-histone complex (DNH) which in turn correlates with a great reduction in number of template regions available for transcription. This is suggested by (*a*) the progressive stabilization of the bull spermatid genome in thermal denaturation experiments (32), (*b*) the decrease in the [^{3}H]actinomycin D binding rate in final spermiogenic steps (7, 11) as indicative of a modification in the DNH (1, 3, 7) interfering with the hydrogen bonding and formation of an actinomycin-deoxyguanosine complex (13), and (*c*) reduced binding capacity for cationic dyes due to a

reduction in the number of available negatively charged phosphate groups in the late spermatid DNH (32).

We wish to acknowledge our indebtedness to Dr. H. Stanley Bennett for his support and continuous interest. We are also very grateful to Dr. Oscar L. Miller, Jr. for stimulating discussion and advice as well as for making available to us original micrographs of *Escherichia coli* active genomes. We thank Mr. Yukio Tanaka for providing the electron microscope negative of copper phthalocyanine crystal lattice and for his skilled technical assistance.

This work was presented at the 14th annual meeting of the American Society for Cell Biology, San Diego, Calif., 1974 (*J. Cell Biol.* 1974. **63**(2, Pt. 2): 167 a. Abstr.).

This work was supported by a grant from The Rockefeller Foundation to the Laboratories for Reproductive Biology, University of North Carolina, Chapel Hill, N. C.

Received for publication 18 November 1974, and in revised form 20 January 1975.

REFERENCES

1. BARCELLONA, W. J., R. B. BRACKEEN, and B. R. BRINKLEY. 1974. Differential binding of tritiated actinomycin to the nuclei of mammalian spermatogenic cells *in vivo*. *J. Reprod. Fertil.* **39**:41–48.
2. BLOCH, D. P. 1969. A catalog of sperm histones. *Genetics* (*Suppl*). **61**:93–111.
3. BRACHET, J., and N. HULIN. 1969. Binding of tritiated actinomycin and cell differentiation. *Nature* (*Lond.*). **222**:481–482.
4. BURGOS, M. H., and D. W. FAWCETT. 1955. Studies on the fine structure of the mammalian testis. I. Differentiation of the spermatids in the cat. *J. Biophys. Biochem. Cytol.* **1**:287–300.
5. CALVIN, H. I., and J. M. BEDFORD. 1971. Formation of disulphide bonds in the nucleus and accessory structures of mammalian spermatozoa during maturation in the epididymis. *J. Reprod. Fertil.* (*Suppl*). **13**:65–75.
6. COELINGH, J. P., T. H. ROZIJN, and C. H. MONFOORT. 1969. Isolation and partial characterization of basic protein from bovine sperm heads. *Biochim. Biophys. Acta.* **188**:353–356.
7. DARZYNKIEWICZ, Z., B. L. GLEDHILL, and N. R. RINGERTZ. 1969. Changes in deoxyribonucleoprotein during spermiogenesis in the bull. ^{3}H-Actinomycin D binding capacity. *Exp. Cell Res.* **58**:435–438.
8. DIXON, G. H., C. J. INGLES, B. JERGIL, V. LING, and K. MARUSHIGE. 1968. Protein transformations during differentiation of trout testis. *Proc. Can. Cancer Res. Conf.* **8**:76–102.
9. FAWCETT, D. M., and D. PHILLIPS. 1970. Recent observations on the ultrastructure and development of the mammalian spermatozoon. Proceedings of the First International Symposium on Comparative Spermatology. Academia Nazionale dei Lincei. Rome.
10. GALDIERI, M., and V. MONESI. 1973. Ribosomal RNA synthesis in spermatogonia and Sertoli cells of the mouse testis. *Exp. Cell Res.* **80**:120–126.
11. GLEDHILL, B. L., Z. DARZYNKIEWICZ, and N. R. RINGERTZ. 1971. Changes in deoxyribonucleoprotein during spermiogenesis in bull: increased [^{3}H]-actinomycin D binding to nuclear chromatin of morphologically abnormal spermatozoa. *J. Reprod. Fertil.* **26**:25–38.
12. HAMKALO, B. A., and O. L. MILLER, JR. 1973. Electron microscopy of genetic activity. *Annu. Rev. Biochem.* **42**:379–396.
13. JAIN, S. C., and H. M. SOBELL. 1972. Stereochemistry of actinomycin binding to DNA. I. Refinement and further structural details of the actinomycin-deoxyguanosine crystalline complex. *J. Mol. Biol.* **68**:21–34.
14. KIERSZENBAUM, A. L. 1974. RNA synthetic activities of Sertoli cells in the mouse testis. *Biol. Reprod.* **11**:365–376.
15. KIERSZENBAUM, A. L., and L. L. TRES. 1974. Nucleolar and perichromosomal RNA synthesis during meiotic prophase in the mouse testis. *J. Cell Biol.* **60**:39–53.
16. KIERSZENBAUM, A. L., and L. L. TRES. 1974. Transcriptional sites in spread meiotic prophase chromosomes in the mouse testis. *J. Cell Biol.* **63**:923–935.
17. KISTLER, W. S., M. E. GEROCH and H. G. WILLIAMS-ASHMAN. 1973. Specific basic proteins from mammalian testes. *J. Biol. Chem.* **248**:4532–4543.
18. KORNBERG, R. D. 1974. Chromatin structure: a repeating unit of histones and DNA. *Science* (*Wash. D.C.*). **184**:868–871.
19. LAM, D. M. K., and W. R. BRUCE. 1971. The biosynthesis of protamine during spermatogenesis of the mouse: extraction, partial characterization and site of synthesis. *J. Cell Physiol.* **78**:13–24.
20. LUNG, B. 1968. Whole-mount electron microscopy of chromatin and membranes in bull and human sperm heads. *J. Ultrastruct. Res.* **22**:485–493.
21. LUNG, B. 1972. Ultrastructure and chromatin disaggregation of human sperm head with thioglycolate treatment. *J. Cell Biol.* **52**:179–186.
22. MARUSHIGE, Y., and K. MARUSHIGE. 1974. Properties of chromatin isolated from bull spermatozoa. *Biochim. Biophys. Acta.* **340**:498–508.

23. MARUSHIGE, Y., and K. MARUSHIGE. 1975. Transformation of sperm histone during formation and maturation of rat spermatozoa. *J. Biol. Chem.* **250:** 39–45.
24. MILLER, O. L., and A. H. BAKKEN. 1972. Morphological studies of transcription. *Acta Endocrinol. (Suppl.)* **168:**155–177.
25. MONESI, V. 1964. Autoradiographic evidence of a nuclear histone synthesis during mouse spermiogenesis in the absence of detectable quantities of nuclear ribonucleic acid. *Exp. Cell Res.* **36:**683–688.
26. MONESI, V. 1965. Differential rate of ribonucleic acid synthesis in the autosomes and sex chromosomes during male meiosis in the mouse. *Chromosoma (Berl.).* **17:**11–21.
27. MOORE, G. P. M. 1971. DNA-dependent RNA synthesis in fixed cells during spermatogenesis in the mouse. *Exp. Cell Res.* **68:**462–465.
28. NOLL, M. 1974. Subunit structure of chromatin. *Nature (Lond.).* **251:**249–251.
29. OAKBERG, E. F. 1956. A description of spermiogenesis in the mouse and its use in analysis of the cycle of the seminiferous epithelium and germ cell renewal. *Am. J. Anat.* **99:**391–413.
30. OLINS, A. L., and D. E. OLINS. 1974. Spheroid chromatin units (ν bodies). *Science (Wash. D. C.).* **183:**330–332.
31. PHILLIPS, D. M. 1970. Insect sperm: their structure and morphogenesis. *J. Cell Biol.* **44:**243–277.
32. RINGERTZ, N. R., B. L. GLEDHILL, and Z. DARŻYNKIEWICZ. 1970. Changes in deoxyribonucleoprotein during spermiogenesis in the bull. Sensitivity of DNA to heat denaturation. *Exp. Cell Res.* **62:**204–218.
33. SALPETER, M. M., and L. BACHMANN. 1972. Autoradiography. *In* Principles and Techniques of Electron Microscopy. Biological Applications. Vol. 2. M. A. Hayat, editor. Van Nostrand Company, Inc., D., New York. 221–278.
34. SALPETER, M. M., and M. SZABO. 1972. Sensitivity in electron microscope autoradiography using Ilford L4 emulsion: the effect of radiation dose. *J. Histochem. Cytochem.* **20:**425–434.
35. SILVERMAN, L., and D. GLICK. 1969. The reactivity and staining of tissue proteins with phosphotungstic acid. *J. Cell Biol.* **40:**761–767.
36. UTAKOJI, T. 1966. Chronology of nucleic acid synthesis in meiosis of the male Chinese hamster. *Exp. Cell Res.* **42:**585–596.
37. WORCEL, A., E. BURGI, J. ROBINTON, and C. L. CARLSON. 1973. Studies on the folded chromosome of *Escherichia coli*. *Cold Spring Harbor Symp. Quant. Biol.* **38:**43–51.
38. ZIRKIN, B. R. 1971. The fine structure of nuclei in mature sperm. I. Application of the Langmuir trough-critical point method to histone-containing sperm nuclei. *J. Ultrastruct. Res.* **36:**237–248.